BB

MICHIGAN STATE
UNIVERSITY

National Superconducting Cyclotron Laboratory

PROBING THE SUSTAINABILITY OF THE N = 82 AND Z = 50 SHELL CLOSURES FOR NEUTRON-RICH NUCLIDES: DECAY OF $^{120}Rh_{75}$ TO LEVELS OF $^{120}Pd_{74}$

W.B. WALTERS, B.E. TOMLIN, P.F. MANTICA, B.A. BROWN, J. RIKOVSKA STONE, A.D. DAVIES, A. ESTRADE, P.T. HOSMER, N. HOTELING, S.N. LIDDICK, T.J. MERTZIMEKIS, F. MONTES, A.C. MORTON, W.F. MUELLER, M. OUELLETTE, E. PELLEGRINI, P. SANTI, D. SEWERYNIAK, H. SCHATZ, J. SHERGUR, and A. STOLZ

MSUCL-1288 JULY 2004

INTRODUCTION

The effect of quenching of neutron shell gaps in neutron-rich nuclei has been known in self-consistent mean-field calculations since the late 1970s [1] and has been discussed extensively in a number of publications (see e.g. Ref. [2–4] and references therein). The microscopic origin of the narrowing of neutron shell gaps is found in the interplay between properties of the weakening nucleon-nucleon potential at the nuclear surface and strong pairing effects. The magnitude of the quenching effect is sensitive to the form of the effective nucleon-nucleon interaction. For example, the Skyrme SkP potential predicts quenching independently from the method of treatment of the pairing interaction [2]. For other potentials, pairing plays a decisive role [4]. It follows that the theoretical phenomenon of quenching is a strongly model dependent effect and it is therefore important to seek unambiguous experimental indicators of the shell structure in very neutron-rich nuclei.

The consequence of neutron shell quenching in neutron-rich nuclei in an astrophysical context, first recognized by Haensel *et al.* [5], has been utilized in attempts to understand the significant departures of calculated r-process yields from the observed solar r-process abundances. The key feature, theoretical nuclear masses along the r-process path, depends critically on the underlying shell structure in the region. Amongst many existing mass models, the ETFSI-Q [3], with the quenching introduced analytically into the model, significantly improved the agreement between the calculated r-process yields and observed abundances in the region $112 \leq A \leq 124$ [6].

Dillmann *et al.* [7] recently reported new measurements for the mass of $^{130}\mathrm{Cd}_{82}$ deduced from the experimental β-endpoint energy for the decay $^{130}\mathrm{Cd}_{82} \rightarrow {}^{130}\mathrm{In}_{81}$. They noted that the experimental mass of $^{130}\mathrm{Cd}_{82}$ was higher than expected from some mass model calculations (FRDM [8], ETFSI-1 [9], Duflo-Zuker mass formula [10]) assuming a regular neutron shell closure. On the other hand, the Hartree-Fock-Bogolyubov (HFB) mean field model with SkP Skyrme effective interaction [2] and the ETFSI-Q model with SkSC4 interaction [3] both predict the mass of $^{130}\mathrm{Cd}_{82}$ close to experiment and the neutron "shell quenching" at $N = 82$. Consequently, Dillmann *et al.* [7] proposed that the high Q_β value for $^{130}\mathrm{Cd}_{82}$ was a direct signature of $N = 82$ shell quenching below $^{132}\mathrm{Sn}_{82}$. However, the more recent succession of microscopic mass models, based on either on Hartree-Fock + BCS (HFBCS-1 with MSk7 interation [11]) or HFB (HFB-1 with BSk1 interaction [12] and HFB-2 with BSk2

and BSk2 interactions [4]) methods predict $N = 82$ shell quenching but do not calculate the mass of $^{130}Cd_{82}$ correctly.

Low-energy excited states are also sensitive to shell quenching. In the vicinity of a neutron closed shell, the low-energy yrast excitations in an even-even isotopic sequence are expected to rise with increasing neutron number towards the highest value at the shell closure. Thus the neutron number dependence of the energies of the first 2^+ $[E(2_1^+)]$ and 4^+ $[E(4_1^+)]$ states (usually the only states known experimentally in very exotic nuclei) serves as another important indicator of the presence of shell closures. Experimental data on $E(2_1^+)$ and $E(4_1^+)$ excitations in even-even neutron-rich nuclei with proton number close to $Z = 50$ and neutron number close to $N = 82$ reveal interesting irregularities. For example, Kautzsch *et al.* [13] reported that in $^{128}Cd_{80}$ the values of $E(2_1^+)$ and $E(4_1^+)$ are lower than those for the adjacent nuclide $^{126}Cd_{78}$. Moreover, these energies are significantly different from the corresponding values for the isotonic $_{52}$Te nuclides, $^{130}Te_{78}$ and $^{132}Te_{80}$. Systematics of the known energies of first 2^+ states in even-even $_{48}$Cd nuclides show that the neutron number dependence of $E(2_1^+)$ is not very sensitive to the approaching shell closure at $N = 82$. However, we will point out later that the same effect can be seen in even-even 2-proton-hole $_{80}$Hg isotopes approaching $N = 126$.

On the other hand, recent investigations [14] of the structure of neutron-rich even-even $_{46}$Pd nuclides have shown a similarity with the comparable isotonic $_{54}$Xe energies over much of the known range of neutron numbers and the expected rise in $E(2_1^+)$ towards $N = 82$. Low-energy excited states in even-even $_{46}$Pd isotopes were studied theoretically by Kim *et al.* [15]. The adjustable parameters of this modern IBM calculation are based on the microscopic mapping between multi-nucleon system and interacting boson system [16]. The choice of the model space assumes regular $Z = 50$ and $N = 82$ closed shells. At the time of publication, predictions of low-energy excited state energies up to $^{126}Pd_{80}$ were made, based on experimental values known only up to $^{116}Pd_{70}$. Subsequent study of the β decay of $^{118}Rh_{73}$ to levels of $^{118}Pd_{72}$ [17] revealed that the observed yrast energies up through the 6^+ level were within a few keV of the energies calculated by Kim *et al.* [15] and observed for isotonic $^{126}Xe_{72}$ as shown in Table I. Under conditions where the counting of both neutron and proton bosons is well established, a similar predictive situation was encountered for the structure of $^{142}Xe_{88}$ [18].

We report new data for the levels of $^{120}Pd_{74}$, $^{120}Rh_{75}$, and $^{126}Cd_{78}$. The principal goal of

the investigation was to assess the systematic variation of $E(2_1^+)$ as a function of neutron number for the even-even $_{46}$Pd isotopes as the $N = 82$ closed neutron shell is approached by studying the decay of neutron-rich $_{45}$Rh isotopes to levels of neutron-rich $_{46}$Pd isotopes.

EXPERIMENTAL METHODS

Very neutron-rich $_{45}$Rh nuclides were produced in the fragmentation of a 120-MeV/nucleon $^{136}Xe_{82}$ beam at the National Superconducting Cyclotron Laboratory (NSCL) at Michigan State University. The beam was made incident on 188 mg/cm^2 $_4$Be target and the resulting fragments were separated using the A1900 spectrometer [19] set to rigidities $B\rho_1 = 3.9597$ Tm and $B\rho_2 = 3.8397$ Tm, with a thin plastic degrader placed at the intermediate dispersive image. The momentum acceptance of the spectrometer was limited to 1% to avoid charge states of the $^{136}Xe_{82}$ primary beam. The desired fragments were implanted in the NSCL β counting system [20, 21], which included a 40 mm $\times$ 40 mm $\times$ 1.5 mm thick Double-sided Silicon Strip Detector (DSSD) to correlate implants of known Z and A with subsequent β-decay events. A series of three Si PIN detectors was placed upstream of the DSSD implantation detector to measure the total kinetic energy of the incoming fragments. The β counting system was augmented by 12 detectors from the MSU Segmented Germanium Array (SeGA) [22] allowing the detection of γ rays correlated with both direct implants and subsequent β events in the DSSD. The peak γ-ray efficiency of the array, as configured around the β counting system, was 5.3% at 1.0 MeV.

The particle identification spectrum for those fragments incident on the most upstream Si PIN detector is presented in Fig. 1(a). Due to the difference in ranges of the implanted fragments, not all incident particles reached the DSSD, as shown in Fig. 1(b). The particle identification was complicated by the fact that not all fragments were produced as fully-stripped ions. The presence of charge states in the fragment beam necessitated the determination of the total kinetic energy, as well as the energy-loss and time of flight, to uniquely identify each implant on an event-by-event basis.

An example of the charge-state contamination is given in Fig. 2(a), where the total kinetic energy of fragments corresponding to a gate in the particle identification spectrum on what is expected to be fully-stripped $^{120}Rh_{75}$ ions revealed two peaks. The higher- energy peak has been attributed to $^{120}Rh_{75}^{45+}$, while the peak at lower-energy is from hydrogen-like $^{117}Rh_{72}^{44+}$

ions. The spectrum in Fig. 2(a) included all fragments incident on the most upstream Si PIN detector. If one examines the same total kinetic energy spectrum as in Fig. 2(a), but with the additional requirement that the implanted ions reached the DSSD, then only the more energetic $^{120}Rh_{75}^{45+}$ ions are present, as shown in Fig. 2(b). The range discrimination for the hydrogen-like contaminants was useful in many cases in discriminating against unwanted charge states.

Correlations were made between an identified decay event (consisting of a low-energy signal in both the front and back of DSSD, in anti-coincidence with the upstream Si PIN detectors) and a previous implant in the identical pixel or any of the eight nearest-neighbor pixels. The maximum correlation time between implants and subsequent decay events was limited in software to 1 s. This can be compared to the average time of $\approx$ 100 s between implants in a single pixel of the DSSD.

This same setup also provided for the identification of microsecond nuclear isomers in these neutron-rich fragments. Many of those fragments do not have sufficient energy to reach the DSSD, but stop instead in one of the three upstream Si PIN detectors. As mass and charge are determined by flight time to and energy loss in the first Si PIN detector, isomers can be observed over a much wider range of nuclides than the β-decay correlations, which require implantation into the DSSD. In this experiment, a 20-μs time window for isomeric decay was used. Again, the measurement of total kinetic energy was instrumental in discriminating between fully-stripped and hydrogen-like ions that overlapped in the particle identification spectrum.

RESULTS

The β-delayed γ-ray spectrum gated for $^{120}Rh_{75}$ that was accumulated in 140 hours of running time with an average current of 1.2 pnA of $^{136}Xe_{82}$ is shown in Fig. 3. The most intense line in the spectrum is seen at 438 keV and is assigned to the decay of $^{120}Rh_{75}$. Weaker peaks are seen at 618, 901, and 1123 keV and are also assigned to $^{120}Rh_{75}$ decay. A half-life of 120(10) ms was determined for $^{120}Rh_{75}$ decay (see insert in Fig. 3), based on the difference in absolute times between identified $^{120}Rh_{75}$ fragment implants and their correlated β decays. As the 438-keV γ ray is the most intense in the β-delayed γ-ray spectrum, it is our interpretation that the 438-keV γ ray observed following $^{120}Rh_{75}$ β decay arises from the

2_1^+ to 0_1^+ transition in $^{120}Pd_{74}$. It is unlikely that the 618-keV transition directly populates the ground state of $^{120}Pd_{74}$, as there is no precedent (experimental or theoretical) in the lighter even-even $_{46}$Pd isotopes to have a second excited state so close in energy to the first 2^+ state. The 618-keV γ ray is therefore suggested to populate the proposed 2_1^+ state at 438 keV, and is a candidate for the $4_1^+ \rightarrow 2_1^+$ transition in $^{120}Pd_{74}$. The current data did not contain sufficient statistics to corraborate the tentative assignment of the 618-keV transition using $\gamma\gamma$ coincidences.

In their study of the β decay of $^{118}Rh_{73}$, Jokinen *et al.* [17] reported a total of eight delayed γ rays, all of which we observed in correlation with $^{118}Rh_{73}$ fragments (see Fig. 3). They also noted the presence of β-decaying low- and high-spin isomers in the lighter $_{45}$Rh isotopes, and the possibility of such isomers in the decay of $^{118}Rh_{73}$, owing to the weak (18%) population of the known 6^+ level in $^{118}Pd_{72}$. A single peak at 211 keV was observed in the prompt γ-ray spectrum gated on $^{120}Rh_{75}$ implants as shown in Fig. 4(a). The average flight time for $^{120}Rh_{75}$ fragments from the production target to the β counting system was 860 ns. The observation of an isomeric transition in $^{120}Rh_{75}$ and the apparent absence of population of higher spin states in daughter $^{120}Pd_{74}$ would suggest that the high-spin isomer in $^{120}Rh_{75}$ de-excites via an isomeric transition, rather than via β decay, and that the β decay is from an isomer with lower rather than higher spin.

Isomeric γ rays were also correlated with the implantation of $^{126}Cd_{78}$ fragments as shown in Fig. 4(b). Strong lines at 652, 814, and 401 keV, the same strong lines reported in the decay of $^{126}Ag_{79}$ by Kautzsch *et al.* [13], were observed along with a number of weaker lines. Based on the scatter of points across the accessible range of the time-to-amplitude converter spectrum for the isomeric γ rays assigned to $^{126}Cd_{78}$, the half-life of the $^{126}Cd_{78}$ isomer is most likely longer than the 20 μs time window available for prompt γ-ray detection. There were not enough events from which to derive any coincidence results. However, the large number of γ rays observed suggests a complex decay scheme involving possible high-spin 2-neutron states with spin and parity 7^- and 10^+ as are well-known in isotonic $^{128}Sn_{78}$, as well as possible involvement of the 8^+ 2-proton state. The 401-, 814-, and 652-keV γ rays were placed by Kautzsch *et al.* [23], as arising, respectively, from the cascade from a 5^- level at 1869 keV (1902), through 4^+ level at 1467 keV (1594) through a 2^+ level at 652 keV (740) to the 0^+ ground state in $^{126}Cd_{78}$. The numbers in parentheses are the level position arising from a recent OXBASH calculation [7] for $^{126}Cd_{78}$ and are seen to average about 80 keV

above of the observed positions. The isomeric γ rays recently reported by Hellström *et al.* [24] for $^{125}Cd_{77}$, $^{126}In_{77}$, and $^{127}In_{78}$ were also observed in correlation with those fragments.

DISCUSSION

The proposed new value of $E(2_1^+)$ for $^{120}Pd_{74}$ is displayed in Fig. 5, together with the known $E(2_1^+)$ values in the $_{54}$Xe, $_{52}$Te, $_{48}$Cd, and $_{46}$Pd nuclides. The proposed $E(2_1^+)$ and $E(4_1^+)$ values for $^{120}Pd_{74}$ are shown in Table I, along with previously published 2_1^+ and 4_1^+ energies for $_{46}$Pd and $_{54}$Xe nuclides and the IBM-2 predictions for $^{118}Pd_{72}$ and $^{120}Pd_{74}$. The determination of the $E(2_1^+)$ and $E(4_1^+)$ for $^{118}Pd_{72}$ and $^{120}Pd_{74}$ reveal a extraordinary two-way isotopic symmetry (centered on $^{114}Pd_{68}$) with $^{110}Pd_{64}$ and $^{108}Pd_{62}$ and isotonic symmetry with $^{126}Xe_{72}$ and $^{128}Xe_{74}$, as well as excellent agreement with the earlier IBM-2 calculations of Kim et al. [15].

Given the remarkable proximity of the new $E(2_1^+)$ and $E(4_1^+)$ energies in $^{120}Pd_{74}$ to the calculated energies, to isotopic $^{108}Pd_{62}$, and to isotonic $^{128}Xe_{74}$, we infer that the protons and neutrons in $^{120}Pd_{74}$ nuclide "see" the same $N = 82$ closed neutron shell as is "seen" by isotonic $^{128}Xe_{74}$, as well as the same $Z = 50$ closed proton shell.

Also included in Fig. 5 are the $E(2_1^+)$ values for the 2-proton-hole $_{80}$Hg nuclides and 4-proton hole $_{78}$Pt nuclides just below the $N = 126$ closed shell [25]. What can be seen in these comparisons is that the 4-proton-hole (particle) nuclides, $_{46}$Pd, $_{78}$Pt, and $_{54}$Xe exhibit nuclear structure trends fully consistent with the number of neutron boson holes present a smooth approach to the closed neutron shells. In contrast, $E(2_1^+)$ for the 2-proton-hole (particle) $_{48}$Cd, $_{80}$Hg, and $_{52}$Te nuclides exhibit nuclear structure features that are dominated by shell properties, rather than collective properties. Notice also the divergence for $E(2_1^+)$ in the light $_{52}$Te isotopes as the $N = 50$ closed shell is approached. The relatively good agreement between the 3 observed yrast levels in $^{126}Cd_{78}$ and the positions of those levels calculated within the OXBASH code, truncated by neglecting the contributions of the deep $\pi f_{5/2}$ hole states, is consistent with the notion that shell properties will dominate nuclear structure within 2 particles (holes) of a closed shell, but that collective properties will become increasingly important for nuclides that lie 4 or more particles (holes) away from closed neutron and proton shells. It would be difficult to envision circumstances in which $E(2_1^+)$ and $E(4_1^+)$ for $^{120}Pd_{74}$ could be almost identical to those in isotonic $^{128}Xe_{74}$ and also

be fit, within a few keV, by an IBM-2 calculation which is tuned to fit the whole range of even-even $_{46}$Pd nuclides as a function of the number of neutron bosons, if both the $_{54}$Xe and $_{46}$Pd nuclides did not share almost identical $N = 82$ and $Z = 50$ closed shells. Results of recent mass measurements for the neutron-rich $_{46}$Pd isotopes are, on average, within one standard deviation of the values calculated by the FRDM [26], providing added support for the regular neutron and proton shell closures influencing the low-energy structure of ^{120}Pd. This agreement between measured ground-state masses and the FRDM predictions can be contrasted with the results for ^{130}Cd mentioned earlier [7], where most of the models, including the FRDM, did not adequately reproduce the observed mass.

In conclusion, the new results for the energies of the first 2^+ and 4^+ states in ^{120}Pd$_{74}$ support the notion that the neutron shell quenching is not extended to the $_{46}$Pd nuclei with $N \leq 74$. The proposed impact of a reduced shell gap on r-process waiting points, as the r-process approaches $N = 82$ around $Z = 40 - 42$ is clearly not noticable yet at $Z = 46$. On the other hand, there are hints from the previous experiments for a reduced $N = 82$ shell gap in $N = 78, 80, 82$ isotopes of $_{48}$Cd. More experimental data, especially around $N = 82$ and for $Z \leq 46$ are needed to clarify whether some reduction of the $N = 82$ shell gap occurs in this mass region, and whether it is sufficient to explain the difficulties in many r-process models to reproduce the observed $112 \leq A \leq 124$ abundances in the solar system.

This work was supported in part by the National Science Foundation Grants PHY-01-10253 and PHY-02-44453 and the US Department of Energy Grant DE-FG02-94-ER40834. The authors would like to thank the NSCL operations staff for providing the primary and secondary beams for this experiment. HS is an Alfred P. Sloan Fellow and supported by the National Science Foundation Grant PHY-02-16782 (Joint Institute for Nuclear Astrophysics).

---

[1] T. Tondeur, Z. Phys. A**288**, 97 (1978).

[2] J. Dobaczewski, W. Nazarewicz, T.R. Werner, J.F. Berger, C.R. Chinn, and J. Decharge, Phys. Rev. C**53**, 2809 (1996).

[3] J.M. Pearson, R.C. Nayak, and S. Goriely Phys. Lett. **387**B, 455 (1996).

[4] S. Goriely, M. Samyn, P.H. Heenen, J.M. Pearson, and F. Tondeur, Phys. Rev. C **66**, 024326

(2002).

[5] P. Haensel, J.L. Zudnik, and J. Dobaczewski, Astron. Astrophys. **222**, 353 (1989).

[6] B. Pfeiffer, K.-L. Kratz, F.-K. Thielemann, and W.B. Walters, Nucl. Phys. **A693**, 282 (2001).

[7] I. Dillmann, K.-L. Kratz, A. Wohr, O. Arndt, B.A. Brown, P. Hoff, M. Hjorth-Jensen, U. Koster, A.N. Ostrowski, B. Pfeiffer, D. Seweryniak, J. Shergur, W.B. Walters, and the ISOLDE Collaboration, Phys. Rev. Lett. **91**, 162503 (2003).

[8] P. Möller, J.R. Nix, W.D. Myers, and W.J. Swiatecki, At. Data Nucl. Data Tables **59**, 185 (1995).

[9] Y. Aboussir, J.M. Pearson, A.K. Dutta, and F. Tondeur, At. Data Nucl. Data Tables **61**, 127 (1995).

[10] J. Duflo and A.P. Zuker, Phys. Rev. C **52**, R23 (1995).

[11] S. Goriely, F. Tondeur, and J.M. Pearson, At. Data Nucl. Data Tables **77**, 311 (2001).

[12] M. Samyn, S. Goriely, P.-H. Heenen, J.M. Pearson, and F. Tondeur, Nucl. Phys. **A700**, 142 (2002).

[13] T. Kautzsch, W.B. Walters, M. Hannawald, K.-L. Kratz, V.I. Mishin, V.N. Fedoseyev, W. Bohmer, Y. Jading, P. Van Duppen, B. Pfeiffer, A. Woehr, P. Möller, I. Klockl, V. Sebastian, U. Koester, M. Koizumi, J. Lettry, H.L. Ravn, and the ISOLDE Collaboration, Eur. Phys. J. **A 9**, 291 (2000).

[14] M. Houry, R. Lucas, M.-G. Porquet, Ch. Theisen, M. Girod, M. Aiche, M.M. Aleonard, A. Astier, G. Barreau, F. Becker, J.F. Chemin, I. Deloncle, T.P. Doan, J.L. Durell, K. Hauschild, W. Korten, Y. Le Coz, M.J. Leddy, S. Perries, N. Redon, A.A. Roach, J.N. Scheurer, A.G. Smith, and B.J. Varley, Eur. Phys. J. **A 6**, 43 (1999).

[15] K.-H. Kim A. Gelberg, T. Mizusaki, T. Otsuka, and P. von Brentano, Nucl. Phys. **A604**, 163 (1996).

[16] T. Otsuka, Nucl. Phys. **A557**, 531c (1993).

[17] A. Jokinen, J.C. Wang, J. Aysto, P. Dendooven, S. Nummela, J. Huikari, V. Kolhinen, A. Nieminen, K. Perajarvi, and S. Rinta-Antila, Eur. Phys. J. A**9**, 9 (2000).

[18] A.S. Mowbray, I. Ahmad, Ph. Benet, R.F. Casten, M.P. Carpenter, J.L. Durell, J.B. Fitzgerald, M.A.C. Hotchkis, R.V.F. Janssens, T.L. Khoo, E.F. Moore, L.R. Morss, W.R. Phillips, W. Walters, and D. Ye, Phys. Rev. C **42**, 1126 (1990).

[19] D.J. Morrissey, B.M. Sherrill, M. Steiner, A. Stolz and I. Wiedenhoever, Nucl. Instrum. Meth-

ods Phys. Res. B **204**, 90 (2003).

[20] J.I. Prisciandaro, A.C. Morton, and P.F. Mantica, Nucl. Instrum. Methods Phys. Res. A **505**, 140-143 (2003).

[21] A.C. Morton, Proc. Conference on Application of Accelerators in Research and Industry; AIP Conf. Proc. **680**, 550 (2003).

[22] W.F. Mueller, J.A. Church, T. Glasmacher, D. Gutknecht, G. Hackman, P.G. Hansen, Z. Hu, K.L. Miller, and P. Quirin, Nucl. Instrum. Methods Phys. Res. A **466**, 492 (2001).

[23] T. Kautzsch, W.B. Walters, K.-L. Kratz, and the ISOLDE-IS333-Collaboration, Proc. 2nd International Workshop on Nuclear Fission and Fission-Product Spectroscopy, Seyssins, France; AIP Conf. Proceedings **447**, 183 (1998).

[24] M. Hellström, M.N. Mineva, A. Blahzev, H.J. Boardman, J. Ekman, K. Gladnishki, H. Grawe, J. Gerl, R. Page, Z. Podolyak, D. Rudolph, and the GSI-FRS Isomer Collaboration, *Proceedings of the Third International Conference on Fission and Properties of Neutron-Rich Nuclei*, eds. J.H. Hamilton, A.V. Ramayya, and H.K. Carter, (World Scientific, River Edge, NJ, 2003) p. 22.

[25] M. Caamano, P.H. Regan, Zs. Podolyak, C.J. Pearson, P. Mayet, J. Gerl, Ch. Schlegel, M. Pfützner, M. Hellström, M. Mineva, and the GSI-FRS Isomer Collaboration, Nucl. Phys. **A682**, 223c (2001).

[26] Yu.A. Litvinov *et al.*, GSI Scientific Report 2003, Rep. 2004-1, p. 16.

TABLE I: Experimental 2_1^+ and 4_1^+ energies for $_{46}$Pd and $_{54}$Xe nuclides and the IBM-2 calculated energies for ^{118,120}Pd [15].

Nuclide	$E(2_1^+)$ (keV)	IBM-2 (keV)	$E(4_1^+)$ (keV)	IBM-2 (keV)
$^{108}_{46}Pd_{62}$	434		1046	
$^{120}_{46}Pd_{74}$	438	430	1056	1040
$^{128}_{54}Xe_{74}$	443		1033	
$^{110}_{46}Pd_{64}$	374		921	
$^{118}_{46}Pd_{72}$	379	380	953	900
$^{126}_{46}Xe_{72}$	388		942	

FIG. 1: (Color Online) Particle identification spectrum for (a) all fragments incident on the first Si PIN detector and (b) fragments reaching the DSSD. The intensity scaling in the two-dimensional plot is identical for both (a) and (b). The different isotope patterns reflect the difference in ranges for the implanted isotopes.

FIG. 2: (a) Total kinetic energy spectrum derived by gating on the fragment group representing fully-stripped $^{120}Rh_{75}$ ions in the particle identification spectrum that includes all fragments incident on the first Si PIN detector. The prominent low-energy peak corresponds to hydrogen-like $^{117}Rh_{72}^{44+}$, and the higher-energy tail to fully-stripped $^{120}Rh_{75}^{45+}$. (b) Same as above but with an additional requirement that the fragments reached the DSSD. Only the fully-stripped $^{120}Rh_{75}^{45+}$ ions are present due to stopping of the hydrogen-like contaminant in the upstream Si PIN detectors.

FIG. 3: (a)γ-ray spectrum correlated with the β decay of implanted $^{120}Rh_{75}$ in the range 0 to 2000 keV. The derived decay curve in shown in the inset, where the data were fitted with a function including both parent ($^{120}Rh_{75}$) and daughter ($^{120}Pd_{74}$) decays with a linear background. (b) γ-ray spectrum correlated with the β decay of implanted $^{118}Rh_{73}$ in the range 0 to 1200 keV.

FIG. 4: Isomeric γ rays occuring within a 20-μs time window after implantation of (a) $^{120}Rh_{75}$, and (b) $^{126}Cd_{78}$.

FIG. 5: (Color Online) Energies for the first 2^+ levels in the 2-hole (particle) nuclei $_{52}$Te (open black squares), $_{48}$Cd (open red circles), and $_{80}$Hg (open blue diamonds), and the 4-hole (particle) nuclei $_{54}$Xe (filled black squares), $_{46}$Pd (filled red circles), and $_{78}$Pt (filled blue diamonds). The data for Pd, Cd, Te, and Xe make use of the neutron range $50 < N < 82$, while the data for Hg and Pt are referenced to $114 < N < 126$.

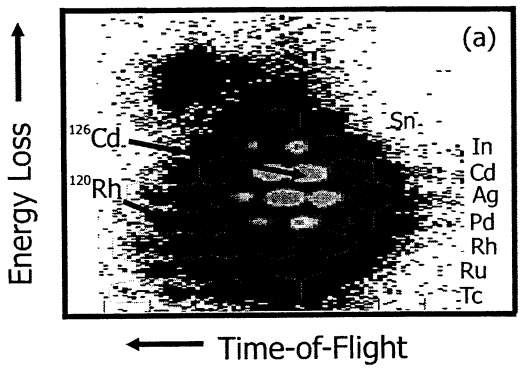
(a)
Energy Loss
^{126}Cd
^{120}Rh
Sn
In
Cd
Ag
Pd
Rh
Ru
Tc
Time-of-Flight

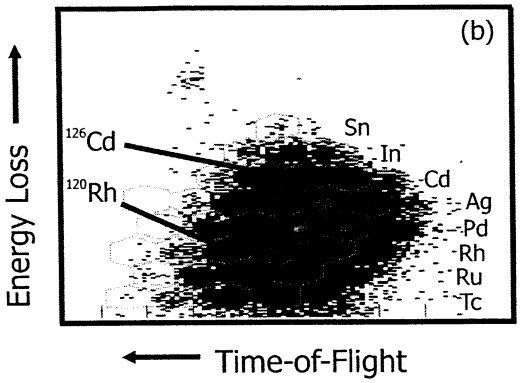
(b)
Energy Loss
126Cd
120Rh
Sn
In
Cd
Ag
Pd
Rh
Ru
Tc
Time-of-Flight

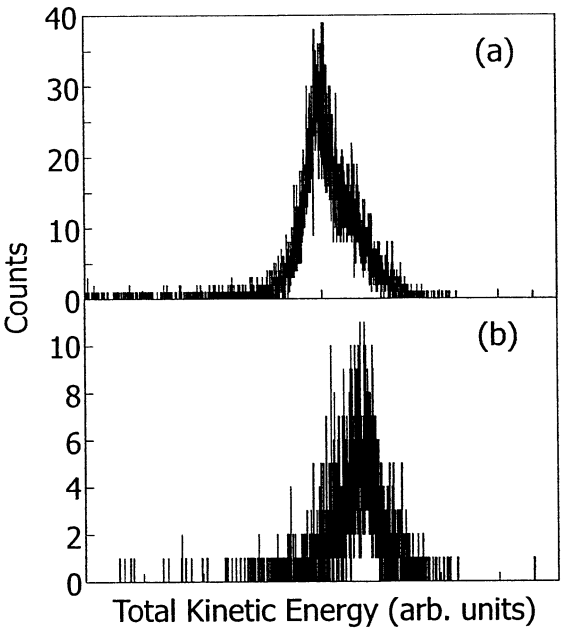
40
30
20
10
0
(a)
10
8
6
4
2
0
(b)
Counts
Total Kinetic Energy (arb. units)

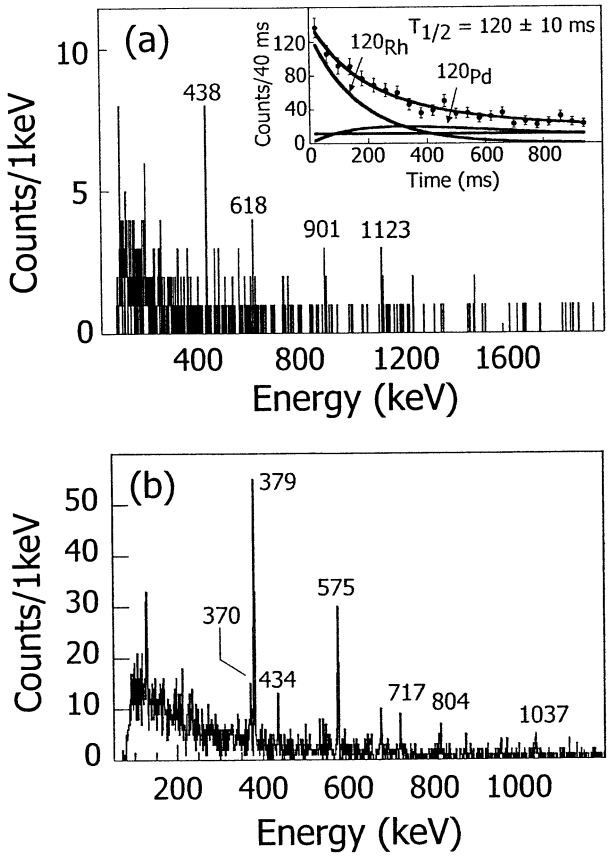
(a)
Counts/1keV
Energy (keV)
438
618
901
1123
$T_{1/2}$ = 120 ± 10 ms
^{120}Rh
^{120}Pd
Counts/40 ms
Time (ms)
(b)
379
575
370
434
717
804
1037

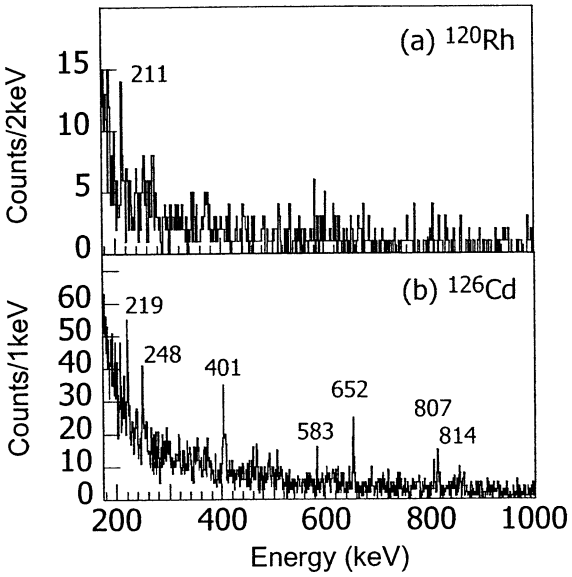
(a) 120Rh
211
Counts/2keV
15
10
5
0
(b) 126Cd
219
248
401
652
807
814
583
Counts/1keV
60
50
40
30
20
10
0
200
400
600
800
1000
Energy (keV)

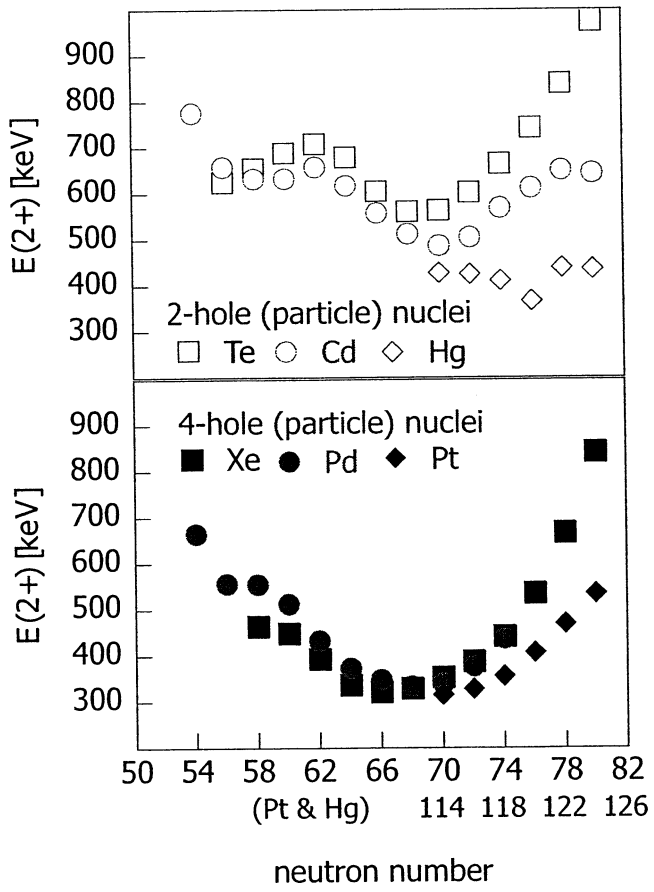
E(2+) [keV]
900
800
700
600
500
400
300
2-hole (particle) nuclei
Te Cd Hg
4-hole (particle) nuclei
Xe Pd Pt
50 54 58 62 66 70 74 78 82
(Pt & Hg) 114 118 122 126
neutron number